PHYSICAL REVIEW B **85**, 060504(R) (2012)

Mass of a vortex in a superconducting film measured via magneto-optical imaging plus ultrafast heating and cooling

Daniel Golubchik,* Emil Polturak, and Gad Koren
Department of Physics, Technion-Israel Institute of Technology, Haifa IL-32000, Israel
(Received 29 October 2011; published 13 February 2012)

We have combined high-resolution magneto-optical imaging with an ultrafast heating and cooling technique to measure the movement of individual vortices in a superconducting film. The motion took place while the film was heated close to T_c, where pinning and viscous forces are relatively small. Under these conditions, vortices move due to the magnetic repulsion between them. We found that a finite vortex mass has to be included in the analysis in order to account for the experimental results. The extent of the motion is consistent with a vortex mass being three orders of magnitude smaller than the mass of all the electrons in the core.

DOI: 10.1103/PhysRevB.85.060504 PACS number(s): 74.25.Ha, 74.25.Gz, 74.25.Uv, 74.40.Gh

Vortices in a superconductor are localized, topologically protected excitations carrying a quantized amount of magnetic flux. They are the "elementary particles" in several models of statistical mechanics (Kosterlitz-Thouless, XY model). One important parameter characterizing a particle is its mass. The size of the mass decides whether vortices are quantum or classical objects.[1] Quantum vortices in unconventional superconductors are predicted to support Majorana excitations[2] and can be applied for quantum computing.[3] A quantized vortex has no intrinsic mass. An effective mass, however, can be associated with its motion. Due to its importance, the concept of the vortex mass was discussed extensively over the years, but remains a controversial issue.[4] One point of view is that mass plays no role in the dynamics since an inertial term in the equation of motion of a vortex is always negligible next to the viscous drag force. Predictions for the value of the mass in different limits (dirty and superclean) span five orders of magnitude.[5–8] Experimentally, the presence of an inertial term is difficult to detect since at low temperatures vortices in superconductors are pinned, and if they move at all, their motion is dominated by viscosity. We are aware of only one such attempt, with inconclusive results.[9] It is quite clear that in order to check if an inertial term plays a significant role in vortex dynamics, one should realize conditions where the viscous drag force is not dominant.

Both pinning[10] and viscous drag forces[11] decrease strongly with temperature and vanish at the critical temperature T_c. In a thin superconducting film, the vortex-vortex interaction ($\mathbf{F}_{\rm int}$) is mainly due to the magnetic field of the vortices outside the film.[12] $\mathbf{F}_{\rm int}$ depends on temperature rather weakly. Consequently, a temperature interval exists near T_c in which the viscous and pinning forces can be smaller than the vortex-vortex interaction, and do not dominate the dynamics. Our experiment was designed to measure vortex motion in this temperature interval. To obtain quantitative estimates, we use a classical equation of motion of a vortex.[7,13] This equation is derived by integrating over the microscopic degrees of freedom, leaving only macroscopic forces:

$$\mu_v d\frac{d\boldsymbol{v}}{dt} = \mathbf{F}_{\rm int} + \mathbf{F}_L - \nabla U_p - \eta\boldsymbol{v}. \qquad (1)$$

Here, μ_v is the vortex mass per unit length, d is the film thickness, $\mathbf{F}_{\rm int}$ is the vortex-vortex interaction, $\mathbf{F}_L \propto \mathbf{J} \times \boldsymbol{\Phi_0}$ is the Lorentz force due to interaction with currents $\mathbf{J}$ (Φ_0 is the flux quantum), U_p is the pinning potential, and $\eta\boldsymbol{v}$ is the viscous drag force. Measurements[14] show that in Nb, the Magnus force[15] is much smaller than the viscous force and can be neglected. In the absence of external currents and fields, the Lorentz force results from currents associated with vortices trapped in the sample. Our observations were performed in a region near the center of the sample where the currents vanish and this force is small.[16]

The vortex-vortex interaction[12] $\mathbf{F}_{\rm int}$ is repulsive for vortices of the same polarity. In the limit $r \gg \lambda$ (λ is the penetration depth), $\mathbf{F}_{\rm int}$ depends on the intervortex spacing r as $F_{\rm int} = \Phi_0^2/\mu_0\pi r^2$. This relation holds even at $0.97T_c$, the maximal temperature where we use it. At this temperature, $\lambda \simeq 0.3\ \mu$m while the minimal $r \sim 1\ \mu$m.

We determined the pinning and the viscous drag forces for our films from transport measurements using the method described by Klein *et al.*[17] The temperature dependence of the various forces is shown in Fig. 1. In the interval between $T^* \approx 0.95T_c$ and T_c, $\mathbf{F}_{\rm int}$ is larger than the viscous drag force. Our experiment was performed in this interval.

The sample is a 200-nm-thick niobium film with T_c of 8.8 K deposited on a sapphire substrate capped by a 50-nm-thick layer of aluminium to increase reflectivity. The film is patterned into squares of 400 μm × 400 μm. The experiment is shielded by μ-metal from external magnetic fields. Small fields (<mT) are applied using a solenoid inside the shield. The vortices in the film are imaged using high-resolution magneto-optics.[18] Using 10 s integration time, our system images large areas of 100 × 100 μm^2 with a 0.8-μm resolution.

Since the typical velocity of a vortex[19] is few km/s, it traverses the field of view in several nanoseconds. No technique can image this motion in real time. Our approach is to take a pinned vortex array, release the pinning for about 1 ns, allowing the vortices to move under the various forces, and then restore the pinning. Pinning can be turned off and on by rapidly heating and cooling the film, as illustrated in the inset of Fig. 1. During the short infrared laser pulse, the temperature of the film is increased from the base temperature of 5.5 K by an amount proportional to the intensity of the light. The 1-mm-thick sapphire substrate is transparent at the wavelength of the laser. Hence, by back-side illumination, only the film heats up, while the substrate remains near the base temperature.

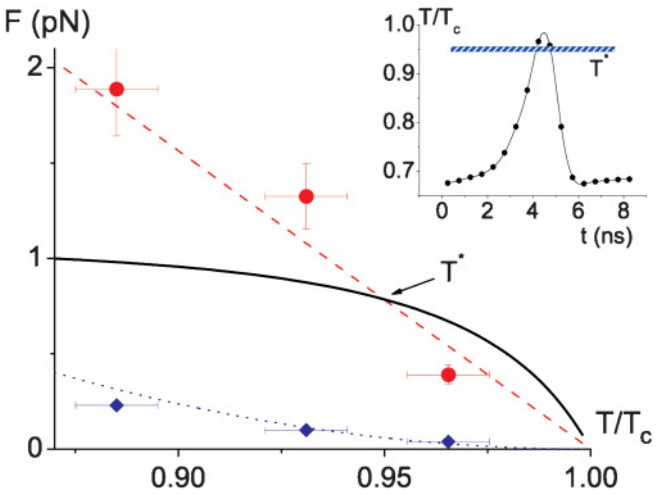

FIG. 1. (Color online) Temperature dependence of the forces acting on a vortex. The quantitative values are for a 200-nm Nb/50-nm Al film. Solid black line is $\mathbf{F}_{\rm int}$ for two vortices separated by 1 μm. Circles (red) show the maximal drag force taken from our transport measurements. Dashed line (red) is a linear fit. Blue diamonds and dotted line represent the measured pinning force and the fit to $F_p(T) = F_p(0)(1 - T/T_c)^2$. T^* is the crossover temperature above which the pinning and the drag force are weaker than $F_{\rm int}$ and vortices are able to move. The inset shows the time dependence of the temperature of the film during a heating pulse. Motion of vortices takes place only during the short-time interval where the temperature exceeds T^*.

Heat escapes from the film via ballistic phonons crossing into the cold substrate. The substrate, which acts as a heat sink, has a thermal mass about 1000 times larger than that of the film, and so its temperature does not increase significantly during the pulse. The thermalization time constant of the film is $\sim 6 \times 10^{-11}$ s, so essentially the film remains hot as long as the laser pulse is on, with its instantaneous temperature proportional to the light intensity. We confirmed this scenario by comparing the temperature profile measured directly using a GeAu thin-film bolometer. The laser pulse intensity profile was measured simultaneously using a fast photodiode. In our apparatus, the length of the heating pulse is fixed, producing a temperature profile shown in the inset of Fig. 1. The static positions of vortices are imaged before and after the motion took place.

Our initial vortex configuration contains small aggregates only a few vortices each, shown in Fig. 2. To prepare such aggregates, we first cool the film in a very small field, typically 30 μT. The field is turned off at low temperature, leaving vortices trapped in the film. We then apply an inhomogeneous heating light pulse. The speckle pattern of the light creates an inhomogeneous illumination, strong enough to increase the temperature above T_c in some small regions. Some of the vortices escape into these normal regions and become trapped as classical flux. Upon cooling, these regions become superconducting again and the trapped flux disintegrates into small aggregates of several vortices each. The typical distance between nearby vortices in an aggregate is ≈ 1 μm. Typically, the aggregates are separated by ~ 10 μm, with the area in-between largely free of vortices.

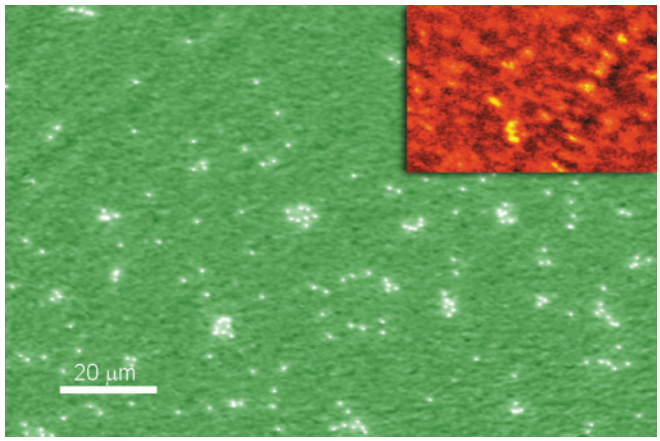

FIG. 2. (Color online) Typical magneto-optical image of vortex aggregates in the superconducting film. Each white spot is an individual vortex. Inset: Light intensity distribution of a typical inhomogeneous laser heating pulse. Bright regions represent high-intensity regions, where the temperature during the pulse is above T_c.

We next apply a homogeneous heating pulse to the film containing the initial vortex array shown in Fig. 2. To obtain uniform illumination (and heating), the light pulse from Nd:YIG laser was passed trough a diffuser. The random intensity variability across the sample translated to temperature units was less then $0.01T_c$. The displacement of vortices can be seen in the differential image shown in Fig. 3, generated by subtracting the image before the pulse from the image after. If the maximal temperature during the pulse does not reach $\sim 0.95T_c$, we see no motion within our resolution. Once the maximal temperature during the pulse exceeded $\sim 0.95T_c$, the aggregates begin to disperse [shown in Fig. 3(a)]. This temperature is in good agreement with T^* estimated using our transport measurements (see Fig. 1). At $T = 0.97T_c$, the typical displacement of the vortices is several μm [see

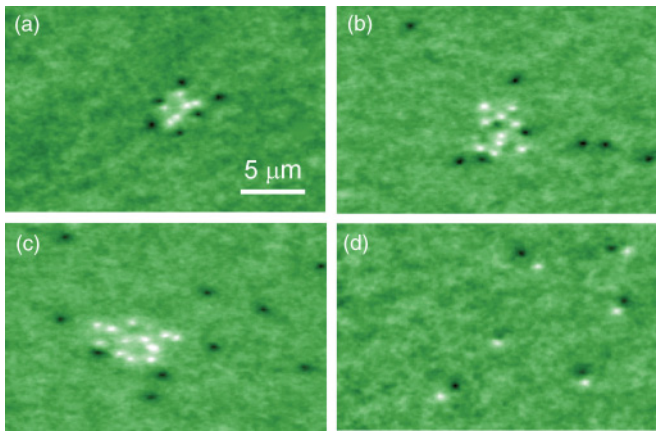

FIG. 3. (Color online) Differential images of typical aggregates of vortices before and after a homogeneous heating pulse. White and dark spots mark the positions of the vortices before and after the pulse. The scale bar for all the panels is the same. (a) An aggregate heated to $T_{\rm max} \simeq 0.95T_C$. (b) An aggregate heated to $T_{\rm max} \simeq 0.97T_C$. (c) An aggregate heated to $T_{\rm max} \simeq 0.99T_C$. (d) Isolated vortices heated to $T_{\rm max} \simeq 0.97T_C$.

Fig. 3(b)]. At $T = 0.99T_c$ [Fig. 3(c)], the displacement becomes comparable to the distance between aggregates. All the trapped vortices disappear at T_c.

An important check involves the displacement of isolated vortices. At $T_{\max} = 0.95T_c$, isolated vortices do not move. At $T_{\max} = 0.97T_c$ [Fig. 3(d)], the displacement is significantly smaller than that of vortices that are part of an aggregate [Fig. 3(b)]. This confirms that within an aggregate, the dominant force is the vortex-vortex interaction ($\mathbf{F}_{\rm int}$) rather than a force exerted by currents, which should affect isolated vortices in the same way as those in aggregates. Along the same lines, once the vortices have dispersed, the intervortex repulsion $\mathbf{F}_{\rm int}$ decreases to the point where even if we heat the film, again the vortices do not move.

When inspecting images taken at $T = 0.97T_c$ [Fig. 3(b)], we can associate individual vortices at their final positions with a particular initial aggregate, while at $T = 0.99T_c$, this is not possible [Fig. 3(c)]. We therefore use only the data at $T = 0.97T_c$ for quantitative analysis. Even within a specific aggregate, it is not straightforward to establish which of the vortices in the initial state is which in the final state. We therefore chose to evaluate the probability that a vortex is displaced by a distance r, assuming that the displacement is minimal. We start with a differential image of the whole field of view, which typically includes ~200 vortices. We then measure all the distances between each of the the vortices in the initial state and all those in a final state. From this data set, we take the shortest distance connecting two vortices, one in the initial state and one in the final state. These two vortices are then removed from the list and the process is repeated. This step is done to avoid double counting. The results were averaged over 8 images with ~1600 vortices in total. Dividing by the total number of vortices gives the probability density $P_{\rm exp}(r)$. The algorithm works well as long as the the vortices do not move further than a typical distance between the initial aggregates, which is true for data obtained at $T = 0.97T_c$.

To compare the experiment with theory, we generate images similar to Fig. 3 by numerical integration of the equation of motion [Eq. (1)]. We start with initial configuration of typically 200 vortices taken from experiment (e.g., Fig. 2). The integration was performed simultaneously on all the vortices. The time dependence of the temperature during the integration was taken from the experiment (shown in the inset of Fig. 1). At each step, $F_{\rm int}$ was calculated using the instantaneous positions of the vortices. Inside an aggregate, the initial value of $F_{\rm int}$ is of the order of 10^{-12} N. The pinning force at each temperature F_p was taken from our transport measurements. F_p, shown in Fig. 1, is consistent with previous measurements on Nb films.[20] At $T \sim 0.95T_c$, for our film thickness $F_p \simeq 6 \times 10^{-14}$ N, more than an order of magnitude smaller than $F_{\rm int}$.

The explicit form of the drag force $\eta \boldsymbol{v}$ is given by[11]

$$\eta(v)\boldsymbol{v} = \eta(0)\frac{\boldsymbol{v}}{1 + (v/v^*)^2}. \qquad (2)$$

Here, $\eta(0)$ is a sample-dependent parameter, and v^* is a characteristic velocity at which the drag force $\eta \boldsymbol{v}$ has a maximum. The measured maximal drag force as a function of temperature is shown in Fig. 1. Both $\eta(0)$ and v^* were determined for our films from our transport data. The values are consistent with prior measurements on Nb films.[21] Combining

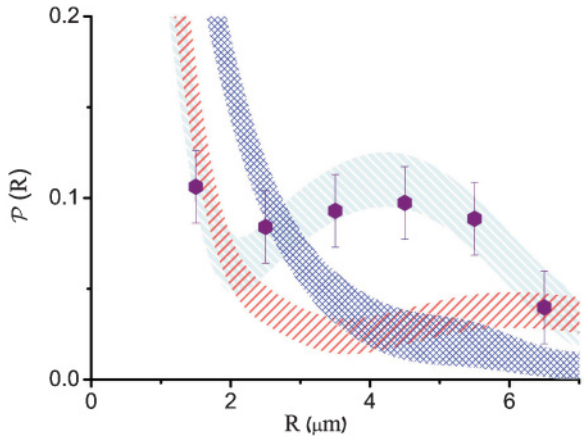

FIG. 4. (Color online) Experimental (solid circles) and calculated (bands) displacement probability distribution of vortices at $T \simeq 0.97T_c$. Dark blue (black) band corresponds to vortex masses of 20 m_e/a, light blue (light gray) band to 5 m_e/a, and red (medium gray) band to 1 m_e/a. The high value of $P(r)$ at small r is largely due to isolated vortices, which move less than 1 μm. The error bars and the width of the bands represent statistical uncertainty.

measured $\eta(0)$ and v^* with the instantaneous velocity v allows us to determine the drag force at each integration step.

The sudden onset of motion at T^* is consistent with the nonlinear form of the viscosity.[11] Vortices are accelerated by $F_{\rm int}$. As long as the velocity is below v^*, the drag force increases with v and the motion is highly damped, limiting the distance traveled to less than 1 μm. At temperatures above T^*, ηv^* becomes smaller than $F_{\rm int}$. A vortex can be accelerated to $v > v^*$, experiences a reduced drag force, and travels distances significantly larger than 1 μm.

The accuracy of the simulations is limited by the experimental uncertainty in the initial positions of the vortices that set the exact value and direction of $F_{\rm int}$. For that reason, the simulations can not reproduce exactly the experimental images. We found, however, that the range of the motion of vortices, which is important to define $P_{\rm sim}(r)$, is unaffected by this uncertainty. To summarize, the pinning force turns out to be small, while the maximal viscous force ηv^* and $F_{\rm int}$ are comparable. We emphasize that with all the forces known, the vortex mass is the only free parameter in the calculation.

Using the initial positions from the experiment and final positions from the simulations, we calculated $P_{\rm sim}(r)$ by the same algorithm described above. Similarly, $P_{\rm sim}(r)$ was averaged over 16 different images. The simulated and experimental $P(r)$ are compared in Fig. 4. The mass per unit length is given in units of electronic mass m_e per lattice constant a. In simulations using large masses ($\mu_v > 20m_e/a$), the vortices move little ($r < 2$ μm) and $P_{\rm sim}(r)$ is large only at small distances. For very small masses ($\mu_v < 1m_e/a$), the displacement can be large and $P_{\rm sim}(r)$ is significant at very large distances. Only for masses $5 < \mu_v < 10$, $P_{\rm sim}(r)$ is large for $2 < r < 5$ μm, which is in good agreement with experiment. This agreement suggests that in the temperature window close to T_c, Eq. (1) can successfully describe the dynamics of vortices. Furthermore, the results are sensitive to the presence of an inertial term. Taking into account all the experimental uncertainties, our final result is $1 < \mu_v < 20$.

Most of the literature quotes the vortex mass at $T = 0$. The calculation of the vortex mass by Suhl[5] relied on the velocity dependence of the free energy of the vortex core. This gave a mass per unit length $\mu_v \sim 1 m_e/a$. Additional contributions to the mass so defined were discussed by several authors.[6] Another approach is to define the mass through the proportionality between the force acting on a vortex and its acceleration.[1,7,8] The resulting mass is of the order of the mass of all the electrons within the vortex core. To compare with our results, we need the value close to T_c. Suhl used the Ginzburg-Landau formalism,[5] valid near T_c. For Nb at $T \simeq 0.97 T_c$ Suhl's mass is $\mu_v \sim 10^{-2} m_e/a$. In the approach involving dynamic response,[1,8] the temperature dependence of the mass was calculated by Han.[7] At $T \simeq 0.97 T_c$, the mass is $\sim 2 \times 10^4 m_e/a$. Our result falls in-between these values. The only other reported measurement[9] comes from the response of a vortex array to sound waves. In a large crystal, the vortices are tangled and the response of the array is collective. This may explain why the reported mass is two orders of magnitude larger even than the largest theoretical prediction. In our experiment, we use low-density vortices in a thin film. At low density, vortices are not entangled, so the dynamic response is that of a single vortex.

It was suggested that the vortex mass depends on the "cleanliness" of the superconductor.[22] Suhl's prediction corresponds to the dirty limit, while the dynamic response prediction corresponds to the superclean limit. Our sample is intermediate between these limits [mean-free path ($l \approx 20$ nm) roughly equals the correlation length ($\xi_0 \approx 40$ nm)]. In conclusion, we have demonstrated that the inertial mass of a vortex is a meaningful concept, which appreciably influences the dynamics close to T_c. "Quantum" vortices may indeed exist in the dirty limit of high-T_c superconductors.

We thank O. Auslaender, E. Zeldov, A. Auerbach, and E. Sonin for illuminating discussions, and E. Buks and S. Hoida for their contributions. This work was supported by the Israel Science Foundation, and by the Minerva and DIP projects.

*danielg@tx.technion.ac.il

[1] G. E. Volovik, Pisma v JETF **65**, 201 (1997) [JETP Lett. **65**, 217 (1997)]; P. Ao and D. J. Thouless, Phys. Rev. Lett. **72**, 132 (1994); G. Blatter, V. B. Geshkenbein, and V. M. Vinokur, *ibid.* **66**, 3297 (1991).

[2] G. E. Volovik, Pisma v JETF **70**, 601 (1999) [JETP Lett. **70**, 609 (1999)].

[3] A. Yu. Kitaev, Ann. Phys. (NY) **303**, 2 (2003); C. Weeks, G. Rosenberg, B. Seradjeh, and M. Franz, Nat. Phys. **3**, 796 (2007).

[4] D. J. Thouless and J. R. Anglin, Phys. Rev. Lett. **99**, 105301 (2007).

[5] H. Suhl, Phys. Rev. Lett. **14**, 226 (1965); M. Yu. Kupriyanov and K. K. Likharev, Zh. Eksp. Teor. Fiz. **68**, 1506 (1975) [Sov. Phys.–JETP **41**, 755 (1975)].

[6] E. M. Chudnovsky and A. B. Kuklov, Phys. Rev. Lett. **91**, 067004 (2003); M. W. Coffey and J. R. Clem, Phys. Rev. B **44**, 6903 (1991); J. M. Duan and A. J. Leggett, Phys. Rev. Lett. **68**, 1216 (1992).

[7] J. H. Han, J. S. Kim, M. J. Kim, and P. Ao, Phys. Rev. B **71**, 125108 (2005).

[8] N. B. Kopnin and V. M. Vinokur, Phys. Rev. Lett. **81**, 3952 (1998).

[9] V. D. Fil, T. V. Ignatova, N. G. Burma, A. I. Petrishin, D. V. Fil, and N. Yu. Shitsevalova, Fiz. Niz. Temp. **33**, 1342 (2007) [Low Temp. Phys. **33**, 1019 (2007)].

[10] S. B. Field, S. S. James, J. Barentine, V. Metlushko, G. Crabtree, H. Shtrikman, B. Ilic, and S. R. J. Brueck, Phys. Rev. Lett. **88**, 067003 (2002).

[11] A. I. Larkin and Yu. N. Ovchinnikov, Zh. Eksp. Teor. Fiz. **68**, 1915 (1976) [Sov. Phys.–JETP **41**, 960 (1976)].

[12] E. H. Brandt, Phys. Rev. B **79**, 134526 (2009).

[13] P. Ao and X. M. Zhu, Phys. Rev. B **60**, 6850 (1999); E. Šimanek, Phys. Lett. A **194**, 323 (1994).

[14] H. Van Beelen and J. P. Van Braam Houckgeest, Physica (Amsterdam) **36**, 241 (1967).

[15] E. B. Sonin, Phys. Rev. B **55**, 485 (1997).

[16] E. Zeldov, J. R. Clem, M. McElfresh, and M. Darwin, Phys. Rev. B **49**, 9802 (1994).

[17] W. Klein, R. P. Huebener, S. Gauss, and J. Parisi, J. Low Temp. Phys. **61**, 413 (1985).

[18] D. Golubchik, G. Koren, E. Polturak, and S. Lipson, Opt. Express **17**, 16160 (2009).

[19] U. Bolz, B. Biehler, D. Schmidt, B. U. Runge, and P. Leiderer, Europhys. Lett. **64**, 517 (2003).

[20] G. S. Park, C. E. Cunningham, B. Cabrera, and M. E. Huber, Phys. Rev. Lett. **68**, 1920 (1992); E. W. J. Straver, J. E. Hoffman, O. Auslaender, D. Rugar, and K. A. Moler, Appl. Phys. Lett. **93**, 172514 (2008).

[21] C. Villard, C. Peroz, and A. J. Sulpice, Low Temp. Phys. **131**, 957 (2003).

[22] E. B. Sonin, V. B. Geshkenbein, A. van Otterlo, and G. Blatter, Phys. Rev. B **57**, 575 (1998).